How to implement constrained mixture growth and remodeling algorithms for soft biological tissues

Lauranne Maes[a,*], Nele Famaey[a]

[a]Biomechanics Section, Department of Mechanical Engineering, KU Leuven, Celestijnenlaan 300 box 2419, 3001 Leuven, Belgium

ARTICLE INFO

Keywords:
Constrained mixture theory
Homogenized constrained mixture theory
Soft tissue biomechanics
Growth and remodeling

ABSTRACT

Biological soft tissues are constantly adapting to their mechanical environment and remodel to restore certain mechanobiological homeostatic conditions. These effects can be modeled using the constrained mixture theory, that assumes degradation of material over time and the gradual replacement of red extant material by newly deposited material. While this theory presents an elegant way to grasp phenomena of growth and remodeling in soft biological tissues, implementation difficulties may arise. Therefore, we give a detailed overview of the mathematical description of the constrained mixture theory and its homogenized equivalent, and present practical suggestions to numerically implement the theories. These implementations are thoroughly tested with multiple example growth and remodeling models. Results show a good correspondence between both theories, with the homogenized theory favored in terms of time efficiency. Results of a step time convergence study show the importance of choosing a small enough time step, especially when using the classical theory.

1. Introduction

Biological soft tissues undergo constant remodeling in order to withstand and respond to changing biomechanical loads. Although the exact cellular processes are unknown, evidence shows that there is a certain mechanobiological homeostatic set-point (or set-region) and that tissue regulatory processes are aimed at restoring this set-point. For example, the tension in and stiffness of the extracellular matrix (ECM) in arteries are similar across species [1, 2], while vascular smooth muscle cells also tend to adapt to a set tension level [3].

The existence of such a homeostatic set-point has inspired several theories of growth and remodeling for biological soft tissues. The constrained mixture theory, as first proposed by Humphrey and Rajagopal [4], assumes that biological tissues are mixtures of multiple constituents, such as elastin and collagen, that can have different natural states and grow (change in mass) and remodel (change in microstructure) at different rates. However, the constituents are constrained to move together in the tissue. The theory relies on one main assumption, namely that every constituent has a preferred mechanical state and is always deposited by the

*Corresponding author
lauranne.maes@kuleuven.be (L. Maes); nele.famaey@kuleuven.be (N. Famaey)
ORCID(s): 0000-0002-1192-0836 (L. Maes); 0000-0002-7374-8912 (N. Famaey)

ECM-producing cells in this preferred condition. For example, a preferred stretch of around 1.1 was found for collagen fibers in the mouse carotid artery [5, 6].

The constrained mixture theory has been used by many research groups for many applications. Humphrey [7] provides an overview of multiple applications in the cardiovascular field. Although the theory is biologically sound and microstructurally motivated, Cyron et al. [8] recognized an important drawback in terms of computational cost. In order to reduce the large required storage space, while preserving the physiological interpretation, they proposed a homogenized version of the constrained mixture theory. They showed that this theory presents the same remodeling behavior in the linear regime and, away from it, a good approximation [8]. This homogenized constrained mixture theory has also been used for various applications, mainly in the cardiovascular biomechanics field [9, 10, 11, 12].

The theoretical concepts regarding the classical and homogenized constrained mixture models have been described in the previously mentioned references. However, practical information about the implementation of these models, as well as public repositories containing these implementations, are very scarce. Nonetheless, this information is crucial in order to efficiently make use of the theory in new applications and to avoid implementation mistakes that often go unnoticed.

Therefore, in the next sections, a detailed theoretical overview is given, followed by a tutorial explaining the practical implementation. Finally, a number of test cases are presented and the model implementations are verified by comparing the results obtained from the constrained mixture theory with the results from the homogenized equivalent. This text is also accompanied by a public repository containing the implementation of the test cases.

Another aim of this work, along with providing readers the necessary information to implement their own models, is to provide a better understanding of the mathematical concepts used in the constrained mixture theory, and their consequences. This is done through thorough discussion of the results of the different test cases.

2. Methods

This section first gives an overview of the theoretical concepts related to the constrained mixture model and its homogenized equivalent. Then, possible practical implementations of these theories are explained, after which a number of test cases are described.

2.1. Constrained mixture model

2.1.1. Remodeling

According to the constrained mixture theory, biological soft tissue is a mixture of different constituents with different mechanical properties and natural configurations, but constrained to move together in the tissue. Each constituent may be constantly degrading and deposited. Therefore, the total mass density of constituent j referred to the reference configuration is [4, 13]

$$\rho^j(s) = \rho_0^j Q^j(s) + \int_0^s m^j(\tilde{\tau}) q^j(s,\tilde{\tau}) d\tilde{\tau}, \tag{1}$$

where ρ_0^j is the total mass density present at the beginning of the remodeling period and $Q^j(s)$ is its remaining fraction at time s. The time-dependent rate of deposition of constituent j is denoted by $m^j(\tilde{\tau})$ and $q^j(s,\tilde{\tau})$ is the fraction of material deposited at $\tilde{\tau}$, surviving to s.

Assuming that newly deposited material is deposited at a specific prestretch deposition tensor $\boldsymbol{G}^j$, the current elastic part of the deformation gradient at time s of a constituent j, deposited as time τ is [4, 13]

$$\boldsymbol{F}_e^j(s,\tau) = \boldsymbol{F}(s)\boldsymbol{F}^{-1}(\tau)\boldsymbol{G}^j. \tag{2}$$

The tensor $\boldsymbol{F}(s)$ is the current total deformation gradient of the mixture with respect to the reference configuration, often chosen as the mechanical homeostatic configuration of the tissue or the configuration at time zero, as is also the case in the remainder of this work. The tensor $\boldsymbol{F}(\tau)$ represents that same deformation at the time of deposition. Note that in this work, the prestretch deposition tensor $\boldsymbol{G}^j$ is considered constant for a certain constituent j, although it can also be made dependent on the time of deposition τ.

The contribution of each constituent to the total strain energy $\Psi^j(s)$ per unit reference volume is

$$\Psi^j(s) = \rho_0^j Q^j(s) W^j(s,0) + \int_0^s m^j(\tilde{\tau}) q^j(s,\tilde{\tau}) W^j(s,\tilde{\tau}) d\tilde{\tau}, \tag{3}$$

where the strain energy density per unit reference mass of constituent j, $W^j(s,\tau)$, is a function of the elastic part of the deformation gradient $\boldsymbol{F}_e^j(s,\tau)$. The Cauchy stress tensor for the stress contribution of constituent j is then

$$\boldsymbol{\sigma}^j(s) = \frac{1}{\phi^j(s)J(s)} \rho_0^j Q^j(s) \frac{\partial W^j(s,0)}{\partial \boldsymbol{F}(s)} \boldsymbol{F}^T(s) + \frac{1}{\phi^j(s)J(s)} \int_0^s m^j(\tilde{\tau}) q^j(s,\tilde{\tau}) \frac{\partial W^j(s,\tilde{\tau})}{\partial \boldsymbol{F}(s)} \boldsymbol{F}^T(s) d\tilde{\tau}, \tag{4}$$

with $J(s) = \det \boldsymbol{F}(s)$ and $\phi^j(s) = v^j(s)/v^{tot}(s)$ the volume fraction of constituent j with respect to the current total volume $v^{tot}(s) = \sum_j v^j(s)$.

2.1.2. Growth

With equation 2, the classical constrained mixture theory assumes that there is no inelastic growth of the tissue, such that a changing density does not lead to an increased volume. In order to allow comparison with the homogenized constrained mixture theory, volume changes are introduced by adapting equation 2 to

$$\boldsymbol{F}_e^j(s,\tau) = \boldsymbol{F}(s)\boldsymbol{F}_g^{-1}(s)\left[\boldsymbol{F}(\tau)\boldsymbol{F}_g^{-1}(\tau)\right]^{-1}\boldsymbol{G}^j, \tag{5}$$

where the growth deformation gradient $\boldsymbol{F}_g(s)$ at a certain time point s is directly related to the total current mass density of all constituents ($\rho^{tot} = \sum_j \rho^j$) and depends on the growth direction. For isotropic growth [9]

$$\boldsymbol{F}_g = \left(\frac{\rho^{tot}(s)}{\rho^{tot}(0)}\right)^{1/3}\boldsymbol{I}, \tag{6}$$

and for transversely isotropic growth in the referential direction represented with unit vector $\boldsymbol{a}_g$ [9]

$$\boldsymbol{F}_g = \frac{\rho^{tot}(s)}{\rho^{tot}(0)}\boldsymbol{a}_g \otimes \boldsymbol{a}_g + \left(\boldsymbol{I} - \boldsymbol{a}_g \otimes \boldsymbol{a}_g\right). \tag{7}$$

Note that the determinant of the growth deformation gradient is always equal to the relative current total density: $J_g = \det \boldsymbol{F}_g = \rho^{tot}(s)/\rho^{tot}(0)$.

2.1.3. Homeostasis

Assuming a steady exponential degradation of constituent j with a half life period of $\log(2)T^j$, the decay functions $Q^j(s)$ and $q^j(s,\tau)$ may be written as [8]

$$\begin{aligned} Q^j(s) &= \exp\left(\frac{-s}{T^j}\right), \\ q^j(s,\tau) &= \exp\left(\frac{-s+\tau}{T^j}\right), \end{aligned} \tag{8}$$

where T^j represents the characteristic decay time.

During mechanical homeostasis, the rate of deposition of constituent j is equal to its homeostatic deposition rate: $m^j(s) = m_0^j$, while every cohort is subjected to the same homeostatic mechanical loading,

such that $W^j(s,\tau) = W^j(s,0) = W_0^j$. Along with equation 8, equation 3 then becomes

$$\begin{aligned}\Psi^j(s) &= \rho_0^j \exp\left(\frac{-s}{T^j}\right) W_0^j + m_0^j W_0^j \int_0^s \exp\left(\frac{-s+\tilde{\tau}}{T^j}\right) d\tilde{\tau} \\ &= \left[\rho_0^j \exp\left(\frac{-s}{T^j}\right) + m_0^j T^j \left(1 - \exp\left(\frac{-s}{T^j}\right)\right)\right] W_0^j,\end{aligned} \tag{9}$$

such that, in order to sustain homeostasis, it must hold that

$$m_0^j = \frac{\rho_0^j}{T^j}, \tag{10}$$

also noting that ρ_0^j is equal to the initial density $\rho^j(0)$ of constituent j.

2.1.4. Nonhomeostatic growth and remodeling

In case of deviation from homeostasis, for example due to damage to the tissue or an increase in external loading, the rates of material degradation and deposition may vary over time. The rate of deposition of a constituent j can for example be written as a function of the average of a certain scalarized version of the Cauchy stress σ_f^j:

$$m^j(s) = \frac{\rho^j(s)}{T^j}\left(1 + k_{\sigma+}\frac{\sigma_f^j(s) - \sigma_f^j(0)}{\sigma_f^j(0)}\right), \tag{11}$$

where $\sigma_f^j(0)$ in the denominator can be omitted if equal to zero. Also assuming a stress-dependent rate of degradation, $Q^j(s)$ and $q^j(s,\tau)$ can be written as

$$\begin{aligned}Q^j(s) &= \exp\left(-\int_0^s K_-^j(\tilde{\tau})d\tilde{\tau}\right) \\ q^j(s,\tau) &= \exp\left(-\int_\tau^s K_-^j(\tilde{\tau})d\tilde{\tau}\right)\end{aligned} \tag{12}$$

where for example

$$K_-^j(s) = \frac{1}{T^j}\left(1 + k_{\sigma-}\frac{\sigma_f^j(s) - \sigma_f^j(0)}{\sigma_f^j(0)}\right), \tag{13}$$

or without denominator if $\sigma_f^j(0)$ is zero.

2.2. Homogenized constrained mixture model

2.2.1. Remodeling

The use of the constrained mixture theory is computationally expensive. Therefore, in the homogenized constrained mixture theory, a computationally efficient approximation proposed by Cyron et al. [8], the different contributions of the cohorts of a constituent deposited at different time points are homogenized. The change of density of a constituent at time point s is written as the sum of the rate of deposition and rate of degradation:

$$\dot{\rho}^j(s) = \dot{\rho}^j_+(s) + \dot{\rho}^j_-(s). \tag{14}$$

Inspired by the kinematic growth theory by Rodriguez et al. [14], Cyron et al. [8] write the elastic part of the deformation gradient of j as

$$\boldsymbol{F}^j_e(s) = \boldsymbol{F}(s)\boldsymbol{F}_g(s)^{-1}\boldsymbol{F}^j_r(s)^{-1}. \tag{15}$$

Note that this deformation gradient is independent of the time of deposition and holds for the constituent j as a whole. The tensor $\boldsymbol{F}^j_r(s)$ is the remodeling deformation gradient that takes into account the inelastic deformation due to mass turnover, accounting for the difference between stretch states of newly deposited and extant material.

In accordance with the constrained mixture theory, Cyron et al. [8] proposed a mass-averaged stress over all cohorts. Therefore, for a constant total deformation gradient $\boldsymbol{F}$ and growth deformation gradient $\boldsymbol{F}_g$, the rate of the Cauchy stress of constituent j for a changing $\boldsymbol{F}^j_r$ is [8]

$$\dot{\boldsymbol{\sigma}}^j_r(s) = -\frac{\dot{\rho}^j_+(s)}{\rho^j(s)}\left(\boldsymbol{\sigma}^j(s) - \boldsymbol{\sigma}^j_{pre}(s)\right), \tag{16}$$

where

$$\begin{aligned}
&\boldsymbol{\sigma}^j(s) = \frac{\rho^i(s)}{\phi^j(s)J(s)}\frac{\partial W^j}{\partial \boldsymbol{F}(s)}\boldsymbol{F}^T(s),\\
&\boldsymbol{\sigma}^j_{pre}(s) = \boldsymbol{R}(s)\boldsymbol{\sigma}^j(0)\boldsymbol{R}(s)^T \quad \text{with} \quad \boldsymbol{F}^j_e(0) = \boldsymbol{G}^j, J(0) = 1, \frac{\rho^i(0)}{\phi^j(0)J(0)} = \frac{M^j_0}{v^j_0},
\end{aligned} \tag{17}$$

where M^j_0/v^j_0 the initial intrinsic mass density of constituent j with M^j_0 the mass and v^j_0 the volume of constituent j at time 0. To compute $\boldsymbol{\sigma}^j_{pre}(s)$, we use $\boldsymbol{\sigma}^j(0)$, since we are looking for the homeostatic Cauchy

stress of constituent j, but then rotated to the current material orientation with $\boldsymbol{R}(s)$. $\boldsymbol{R}(s)$ is an orthonormal tensor representing the rotational part of the deformation gradient, calculated by polar decomposition: $\boldsymbol{F}(s) = \boldsymbol{R}(s)\boldsymbol{U}(s)$, with $\boldsymbol{U}(s)$ the right stretch tensor.

As $\boldsymbol{F}$ and $\boldsymbol{F}_g$ are assumed constant, based on the definition of $\boldsymbol{F}_e^j$ (see equation 15), it also holds that $\boldsymbol{F}_e^j \boldsymbol{F}_r^j$ is constant, such that [8]

$$\dot{\boldsymbol{F}}_e^j = -\boldsymbol{F}_e^j \dot{\boldsymbol{F}}_r^j \left(\boldsymbol{F}_e^j\right). \tag{18}$$

The rate of Cauchy stress can be written in terms of an equivalent rate of elastic part of the deformation gradient. Therefore with equation 18 [8],

$$\dot{\boldsymbol{\sigma}}_r^j(s) = \left(\frac{\partial \boldsymbol{\sigma}^j}{\partial \boldsymbol{F}_e^j} : \dot{\boldsymbol{F}}_e^j\right)_{\boldsymbol{F},\boldsymbol{F}_g=const} = -\left(\frac{\partial \boldsymbol{\sigma}^j}{\partial \boldsymbol{F}_e^j}\right)_{\boldsymbol{F},\boldsymbol{F}_g=const} : \left(\boldsymbol{F}_e^j \dot{\boldsymbol{F}}_r^j \left(\boldsymbol{F}_r^j\right)^{-1}\right). \tag{19}$$

Then with equations 16 and 19 a tensor equation is obtained, from which the rate of the remodeling deformation gradient $\boldsymbol{F}_r^j(s)$ can be determined:

$$\frac{\dot{\rho}_+^j(s)}{\rho^j(s)}\left(\boldsymbol{\sigma}^j(s) - \boldsymbol{\sigma}_{pre}^j(s)\right) = \left(\frac{\partial \boldsymbol{\sigma}^j}{\partial \boldsymbol{F}_e^j}\right)_{\boldsymbol{F},\boldsymbol{F}_g=const} : \left(\boldsymbol{F}_e^j \boldsymbol{L}_r^j\right), \tag{20}$$

with $\boldsymbol{L}_r^j = \dot{\boldsymbol{F}}_r^j \left(\boldsymbol{F}_r^j\right)^{-1}$ the remodeling velocity gradient [8].

2.2.2. Growth

The growth deformation gradient $\boldsymbol{F}_g(s)$ can be calculated in the same way as previously described in section 2.1.2, for example using equation 6 or 7.

2.2.3. Homeostasis

In accordance with equation 10,

$$m_0^j = \dot{\rho}_+^j(0) = \frac{\rho^j(0)}{T^j} \tag{21}$$

in homeostasis. Therefore, in order to maintain homeostasis it should hold that

$$\dot{\rho}_-^j(0) = -\frac{\rho^j(0)}{T^j}, \tag{22}$$

which also follows from equation 8 [8]:

$$\dot{q}^j(s,\tau) = -\frac{q^j(s,\tau)}{T^j}. \tag{23}$$

2.2.4. Nonhomeostatic growth and remodeling

In case of stress-dependent fiber remodeling, in accordance to equations 11 to 13,

$$\begin{aligned}
\dot{\rho}^j_+(s) &= \frac{\rho^j(s)}{T^j}\left(1 + k_{\sigma+}\frac{\sigma^j_f(s) - \sigma^j_f(0)}{\sigma^j_f(0)}\right) \\
\dot{\rho}^j_-(s) &= -\frac{\rho^j(s)}{T^j}\left(1 + k_{\sigma-}\frac{\sigma^j_f(s) - \sigma^j_f(0)}{\sigma^j_f(0)}\right),
\end{aligned} \tag{24}$$

where $\sigma^j_f(0)$ in the denominator can be omitted when equal to zero. Note that by integration of this expression for $\dot{\rho}^j_-(s)$, equivalence with equations 12 and 13 can be shown.

2.3. Constitutive model

As defined earlier, according to the constrained mixture theory, the total mass density of the mixture is the sum of the densities of the constituents j [4]:

$$\rho^{tot} = \sum^{j} \rho^j. \tag{25}$$

The mass averaged total strain energy is then

$$\Psi^{tot} = \sum^{j} \Psi^j, \tag{26}$$

and the total Cauchy stress is calculated as the sum of the contributions of the constituents as

$$\boldsymbol{\sigma}^{tot} = \sum_j \phi^j \boldsymbol{\sigma}^j, \tag{27}$$

where, as defined earlier, $\phi^j = v^j / v^{tot}$ is the volume fraction of the constituent j in the mixture and $\boldsymbol{\sigma}^j$ is defined as in equation 4 or 17 for the constrained mixture and homogenized constrained mixture theories respectively.

The mechanical properties of soft biological tissues, such as arterial tissue, are often modeled taking into account a near-incompressible isotropic ground matrix, representing elastin (elas), reinforced with strain-stiffening collagen (coll) fiber families oriented in different directions i. Therefore, the constitutive functions are written as

$$\begin{aligned} W^{elas} &= C_{10}\left(\bar{I}_1^{elas} - 3\right) + \frac{K}{2}\left(J_e^{elas} - 1\right)^2, \\ W^{coll,i} &= \frac{k_1}{2k_2}\left[\exp\left\{k_2\left(I_4^{coll,i} - 1\right)^2\right\} - 1\right], \end{aligned} \tag{28}$$

where C_{10}, K, k_1 and k_2 are material parameters. The measure for the deformation of the matrix material $\bar{I}_1^{elas}$ is the trace of the deviatoric part of the elastic part of the right Cauchy-Green strain tensor of elastin $\bar{\boldsymbol{C}}_e^{elas} = \left(J_e^{elas}\right)^{-2/3}\left(\boldsymbol{F}_e^{elas}\right)^T \boldsymbol{F}_e^{elas}$, where $\boldsymbol{F}_e^{elas}$ is the elastic part of the deformation gradient of elastin and $J_e^{elas} = \det\left(\boldsymbol{F}_e^{elas}\right)$. The square of the elastic stretch of fiber family i is written as $I_4^{coll,i} = \boldsymbol{M}^i \cdot \left(\boldsymbol{C}_e^{coll,i}\boldsymbol{M}^i\right)$, with $\boldsymbol{C}_e^{coll,i} = \left(\boldsymbol{F}_e^{coll,i}\right)^T \boldsymbol{F}_e^{coll,i}$ and $\boldsymbol{F}_e^{coll,i}$ is the elastic part of the deformation gradient of fiber family i. The direction of fiber family i before elastic deformation is represented by unit vector $\boldsymbol{M}^i$.

In case of a homogeneous elastic part of the deformation gradient, the Cauchy stresses are then, according to the derivation in appendix A,

$$\begin{aligned} \boldsymbol{\sigma}^{elas} &= 2C_{10}\frac{\rho^{elas}}{\phi^{elas}\boldsymbol{J}}\left(\bar{\boldsymbol{B}}_e^{elas} - \frac{1}{3}\bar{I}_1^{elas}\boldsymbol{I}\right) + \frac{K\rho^{tot}}{J_g}\left(J_e^{elas} - 1\right)\boldsymbol{I}, \\ \boldsymbol{\sigma}^{coll,i} &= 2\frac{\rho^{coll,i}}{\phi^{coll,i}\boldsymbol{J}}\frac{\partial W^{coll,i}}{\partial \boldsymbol{I}_4^{coll,i}}\left(\boldsymbol{F}_e^{coll,i}\boldsymbol{M}^i\right) \otimes \left(\boldsymbol{F}_e^{coll,i}\boldsymbol{M}^i\right), \end{aligned} \tag{29}$$

with $\bar{\boldsymbol{B}}_e^{elas} = \left(J_e^{elas}\right)^{-2/3}\boldsymbol{F}_e^{elas}\left(\boldsymbol{F}_e^{elas}\right)^T$ and $J_g = \det\left(\boldsymbol{F}_g\right)$. It holds that $\rho^j/(\phi^j J) = M^j/v^j$ with M^j the current mass of constituent j. Assuming the same relative changes in intrinsic mass density of every constituent, we can state

$$\frac{M^j}{v^j} = \frac{J_g}{J}\frac{M_0^j}{v_0^j}. \tag{30}$$

The scalarized version of the Cauchy stress, as used in equations 11, 13 and 24, can then for example be written as

$$\begin{aligned} \sigma_f^{elas} &= I_{1\sigma}^{elas}, \\ \sigma_f^{coll,i} &= 2\frac{\rho^{coll,i}}{\phi^{coll,i}\boldsymbol{J}}\frac{\partial W^{coll,i}}{\partial \boldsymbol{I}_4^{coll,i}}\boldsymbol{I}_4^{coll,i}, \end{aligned} \tag{31}$$

where $I_{1\sigma}^{elas}$ is the first invariant or trace of the elastin Cauchy stress tensor.

Alternatively, in a fully incompressible formulation,

$$W^{elas} = C_{10}\left(I_1^{elas} - 3\right), \tag{32}$$

where I_1^{elas} is the trace of the right Cauchy-Green tensor of elastin $\boldsymbol{C}_e^{elas} = \left(\boldsymbol{F}_e^{elas}\right)^T \boldsymbol{F}_e^{elas}$. Then

$$\boldsymbol{\sigma}^{elas} = 2C_{10}\frac{\rho^{elas}}{\phi^{elas}}\left(\boldsymbol{B}_e^{elas} - \frac{1}{3}I_1^{elas}\boldsymbol{I}\right), \tag{33}$$

with $\boldsymbol{B}_e^{elas} = \boldsymbol{F}_e^{elas}\left(\boldsymbol{F}_e^{elas}\right)^T$ and in this incompressible case, $\rho^{elas}/\phi^{elas} = M^{elas}/v^{elas} = M_0^{elas}/v_0^{elas}$.

Note that a fully incompressible formulation requires a correction of the diagonal components of the total Cauchy stress tensor through the use of the Lagrange multiplier p, such that $\boldsymbol{\sigma}^{tot} = \sum_j \phi^j \sigma^j - p\boldsymbol{I}$.

2.4. Practical implementation

2.4.1. Constrained mixture model

For the numerical implementation, for example in a user material subroutine of finite element software, the total deformation gradient $\boldsymbol{F}(s)$ is the main input variable, while the total Cauchy stress $\boldsymbol{\sigma}^{tot}(s)$ must be returned. In order to calculate this stress according to the constrained mixture theory, equation 4 needs to be evaluated. To that end, we assume that $s >> 0$, such that $Q^j(s)$ is close to zero and the first term in equation 4 is negligible. To numerically compute the integral, discrete time points τ are considered, separated by Δs. The extant material of a certain constituent is divided into multiple discrete cohorts, depending on the time of deposition τ. A maximal number of cohorts n^j per constituent j are retained to limit the storage space. This number is chosen such that the oldest retained cohort has almost disappeared, according to equation 8. Therefore, for the oldest cohort it holds that $\tau = s - n^j\Delta s$ and all older material is considered negligible with $q^j(s, s-(n^j+1)\Delta s) \approx 0$. Equation 4 then reduces to

$$\boldsymbol{\sigma}^j(s) \approx \frac{1}{\phi^j(s)\boldsymbol{J}(s)}\int_{s-n^j\Delta s}^{s} m^j(\tilde{\tau})q^j(s,\tilde{\tau})\frac{\partial \boldsymbol{W}^j(s,\tilde{\tau})}{\partial \boldsymbol{F}(s)}\boldsymbol{F}^T(s)d\tilde{\tau} \tag{34}$$

For all cohorts τ, the deformation gradient $\boldsymbol{F}(\tau)$ at time of deposition is stored. Moreover, for every cohort of every constituent family, their deposition rate $m^j(\tau)$ at the time of deposition is stored, and potentially the degradation parameter $K_{_}^j(s)$ if time-dependent. Then all necessary information is known

to evaluate equation 34 through numerical integration based on the trapezoidal rule [15] as

$$\boldsymbol{\sigma}^j(s) \approx \frac{\Delta s}{\phi^j(s)\boldsymbol{J}(s)} \sum_{k=1}^{n^j-1} m^j(s-k\Delta s) q^j(s, s-k\Delta s) \frac{\partial \boldsymbol{W}^j(s, s-k\Delta s)}{\partial \boldsymbol{F}(s)} \boldsymbol{F}^T(s) + \frac{\Delta s}{2\phi^j(s)\boldsymbol{J}(s)} \left(m^j(s) \frac{\partial \boldsymbol{W}^j(s,s)}{\partial \boldsymbol{F}(s)} \boldsymbol{F}^T(s) + m^j(s-n^j\Delta s) q^j(s, s-n^j\Delta s) \frac{\partial \boldsymbol{W}^j(s, s-n^j\Delta s)}{\partial \boldsymbol{F}(s)} \boldsymbol{F}^T(s) \right), \tag{35}$$

noting that $q^j(s,s) = 1$.

Equation 1 is evaluated similarly as

$$\rho^j(s) \approx \Delta s \sum_{k=1}^{n^j-1} m^j(s-k\Delta s) q^j(s, s-k\Delta s) + \frac{\Delta s}{2} \left(m^j(s) + m^j(s-n^j\Delta s) q^j(s, s-n^j\Delta s) \right). \tag{36}$$

Note that equations 35 and 36 depend on the current rate of deposition $m^j(s)$, that often depends on the constituent's stress (see for example equation 11). In that case, $m^j(s)$ needs to be calculated iteratively, alternating between equations 4 and 11, since there is likely no closed form solution. It might be tempting to use a left Riemann sum as numerical integration method in order to avoid such an iterative loop. However, due to the exponential nature of the integrated function, this would be too inaccurate for an acceptable step time.

2.4.2. Homogenized constrained mixture model

For the homogenized theory, assuming that the initial density $\rho^j(0)$ of every constituent j is known and by calculating the rate of the density with equation 14 and for example 24, at every time step, the updated density can be calculated with a forward Euler scheme as

$$\rho^j(s+\Delta s) = \rho^j(s) + \dot{\rho}^j(s)\Delta s. \tag{37}$$

Solving equation 20 for $\dot{\boldsymbol{F}}_r^j$ is less straightforward. Although it can be transformed to a set of nine equations with nine unknown tensor elements, these equations are never all independent of each other. Three different cases are discerned.

One-directional fiber family In the first case, assuming a one-directional fiber family, equation 20 can be reduced to a single scalar equation, with a closed form solution for the rate of the remodeling stretch in the

fiber direction. Assuming that the remodeling deformation gradient is

$$\boldsymbol{F}_r^{coll,i} = \lambda_r^{coll,i} \boldsymbol{M}^i \otimes \boldsymbol{M}^i + \frac{1}{\sqrt{\lambda_r^{coll,i}}} \left(\boldsymbol{I} - \boldsymbol{M}^i \otimes \boldsymbol{M}^i \right), \tag{38}$$

with $\lambda_r^{coll,i}$ the remodeling stretch and $\boldsymbol{M}^i$ a unit vector denoting the undeformed direction of the fiber family. Then,

$$\boldsymbol{L}_r^{coll,i} = \frac{\dot{\lambda}_r^{coll,i}}{\lambda_r^{coll,i}} \left(\frac{3}{2} \boldsymbol{M}^i \otimes \boldsymbol{M}^i - \frac{1}{2} \boldsymbol{I} \right). \tag{39}$$

Using the constitutive model of the fiber part of equation 29 and with the help of the derivation in appendix A, we can write in index notation,

$$\begin{aligned} &\left(\frac{\partial \boldsymbol{\sigma}^{coll,i}}{\partial \boldsymbol{F}_e^{coll,i}} \right)_{ijkl}^{\boldsymbol{F}, \boldsymbol{F}_g = const} \\ &= \frac{4\rho^{coll,i}}{\phi^{coll,i} \boldsymbol{J}} \frac{\partial^2 W^{coll,i}}{\left(\partial \boldsymbol{I}_4^{coll,i} \right)^2} \left(\boldsymbol{F}_e^{coll,i} \boldsymbol{M}^i \right)_i \left(\boldsymbol{F}_e^{coll,i} \boldsymbol{M}^i \right)_j \left(\boldsymbol{F}_e^{coll,i} \boldsymbol{M}^i \right)_k \left(\boldsymbol{M}^i \right)_l \\ &+ \frac{2\rho^{coll,i}}{\phi^{coll,i} \boldsymbol{J}} \frac{\partial W^{coll,i}}{\partial \boldsymbol{I}_4^{coll,i}} \left[\delta_{ik} \left(\boldsymbol{F}_e^{coll,i} \boldsymbol{M}^i \right)_j \left(\boldsymbol{M}^i \right)_l + \delta_{jk} \left(\boldsymbol{F}_e^{coll,i} \boldsymbol{M}^i \right)_i \left(\boldsymbol{M}^i \right)_l \right]. \end{aligned} \tag{40}$$

Filling in equations 39 and 40 and projecting equation 20 in the current fiber direction $\boldsymbol{m}^i = \boldsymbol{F}_e^{coll,i} \boldsymbol{M}^i / ||\boldsymbol{F}_e^{coll,i} \boldsymbol{M}^i||$ by performing a double contraction with $\boldsymbol{m}^i \otimes \boldsymbol{m}^i$, we obtain

$$\dot{\lambda}_r^{coll,i} = \frac{\dot{\rho}_+^{coll,i}}{\rho^{coll,i}} \left(\sigma_f^{coll,i} - \sigma_{pre,f}^{coll,i} \right) \frac{\boldsymbol{J} \phi^{coll,i}}{4\rho^{coll,i}} \lambda_r^{coll,i} \left(\frac{\partial^2 W^{coll,i}}{\left(\partial \boldsymbol{I}_4^{coll,i} \right)^2} \left(\boldsymbol{I}_4^{coll,i} \right)^2 + \frac{\partial W^{coll,i}}{\partial \boldsymbol{I}_4^{coll,i}} \boldsymbol{I}_4^{coll,i} \right)^{-1}. \tag{41}$$

This also corresponds to equation 25 in Cyron et al. [8]. An updated version of the remodeling stretch $\lambda_r^{coll,i}$ at every time step is then obtained with a forward Euler method.

Three-dimensional compressible material In the second case, a three-dimensional compressible material is assumed, for example as in the first line of equation 29. Then, according to the derivation in appendix

A,

$$\begin{aligned}
&\left(\frac{\partial \boldsymbol{\sigma}^{elas}}{\partial \boldsymbol{F}_e^{elas}}\right)_{ijkl}^{\boldsymbol{F},\boldsymbol{F}_g=const} \\
=&\frac{2\rho^{elas}}{\phi^{elas}\boldsymbol{J}} C_{10}\left[(\boldsymbol{J}_e^{elas})^{-2/3}\left(\delta_{ik}\left(\boldsymbol{F}_e^{elas}\right)_{jl}+\delta_{jk}\left(\boldsymbol{F}_e^{elas}\right)_{il}-\frac{2}{3}\delta_{ij}\left(\boldsymbol{F}_e^{elas}\right)_{kl}\right)\right. \\
&\left.+\frac{2}{3}(\boldsymbol{J}_e^{elas})^{-2/3}\left(\boldsymbol{F}_e^{elas-T}\right)_{kl}\left(-\left(\boldsymbol{B}_e^{elas}\right)_{ij}+\frac{1}{3}\boldsymbol{I}_1^{elas}\delta_{ij}\right)\right] \\
&+\frac{\rho^{elas}}{\phi^{elas}\boldsymbol{J}_g}K\boldsymbol{J}_e^{elas}\left(\boldsymbol{F}_e^{elas}\right)_{kl}\delta_{ij}
\end{aligned} \tag{42}$$

Due to symmetry of the Cauchy stress, equation 20 contains six independent equations, such that extra assumptions regarding the components of $\boldsymbol{F}_r^j$ are needed. For example, symmetry of $\boldsymbol{F}_r^j$ may be assumed, indicating the absence of a rotational part. The rate of this remodeling deformation gradient is approximated by

$$\dot{\boldsymbol{F}}_r^j = \frac{\boldsymbol{F}_r^j(s+\Delta s)-\boldsymbol{F}_r^j(s)}{\Delta s}. \tag{43}$$

Filling this in and transforming equation 20 to Voigt notation, we obtain a set of six nonlinear equations with as unknowns the six independent components of $\boldsymbol{F}_r^j(s+\Delta s)$ that need to be solved numerically, for example with Newton's method. Our implementation, as can be found in the supplementary material, is largely based on the work of Press et al. [16].

Three-dimensional incompressible material The third case, in which a three-dimensional incompressible material is considered (see equation 33), is very similar. However, the rank of the stiffness tensor, derived according to appendix A,

$$\left(\frac{\partial \boldsymbol{\sigma}^{elas}}{\partial \boldsymbol{F}_e^{elas}}\right)_{ijkl}^{\boldsymbol{F},\boldsymbol{F}_g=const} = 2C_{10}\frac{\rho^{elas}}{\phi^{elas}}\left(\delta_{ik}\left(\boldsymbol{F}_e^{elas}\right)_{jl}+\delta_{jk}\left(\boldsymbol{F}_e^{elas}\right)_{il}-\frac{2}{3}\delta_{ij}\left(\boldsymbol{F}_e^{elas}\right)_{kl}\right) \tag{44}$$

in the Voigt notation version is equal to five, such that only five independent equations remain in the set of equations 20. An extra assumption about $\boldsymbol{F}_r^j$ needs to be made. Naturally, for an incompressible material, we assume a purely isochoric inelastic deformation such that $\det\left(\boldsymbol{F}_r^j\right)=1$.

Model	Constitutive model			Remodeling		Growth	
	matrix incompressible	matrix compressible	fiber	matrix	fiber	matrix	fiber
A	x			x			
B		x		x			
C		x		x		x	
D	x		x		x		
E		x	x		x		x

Table 1
Overview of the tested model implementations. There are three possible constitutive models: incompressible elastin matrix, compressible elastin matrix and collagen fibers. The matrix or the fiber material remodels (changing microstructure), and potentially grows (changing mass). Two versions of all five models (A to E) are implemented, either based on the classical or the homogenized constrained mixture theory.

2.5. Single-element test cases

The models as explained in the previous sections are implemented in user defined material (UMAT) subroutines in the finite element software Abaqus/Standard 2017 (Dassault Systèmes Simulia Corp., Providence Rhode Island, USA). Ten alternative implementations of a growth and remodeling model are tested on three single-element finite element models with different boundary conditions, as explained below. All these different models result in thirty tested cases in total.

The tested model implementations are schematically represented in table 1. All five alternatives are implemented according to the constrained mixture theory and the homogenized equivalent, leading to ten implementations in total. There are three options for the definition of the constitutive model: incompressible elastin matrix material, compressible elastin matrix material and collagen fiber material (see equations 29 and 33). In the latter case, we assume one fiber family in the Y-direction, one in the Z-direction and two symmetrically oriented in the YZ-plane, with an angle α with respect to the Y-axis. These fiber orientations are defined and assumed the same in every integration point of the element. The fiber material is always used in combination with matrix material. Remodeling of either the matrix material or the fibers is assumed, sometimes in combination with growth, assuming anisotropic growth defined with equation 7, where $\boldsymbol{a}_g$ is a unit vector in the X-direction. Note that in Abaqus growth cannot be defined in combination with a hybrid formulation necessary for fully incompressible matrix material. Therefore, this combination is not included in table 1.

These implementations are tested on single-element finite element models in Abaqus. Linear, full integration, hexahedral elements (C3D8) are used, or with an incompressible hybrid formulation (C3D8H) in combination with the incompressible materials of cases A and D defined in table 1. The defined boundary conditions are represented in figure 1. Both XY-planes S3 and S5 are constrained in the Z-direction, one of

the YZ-planes (plane S1) is constrained in the X-direction, one of the XZ-planes (plane S6) is constrained in the Y-direction and a constant Cauchy stress (case S), constant force or first Piola-Kirchhoff stress (case F) or displacement (case U) is applied in the Y-direction on (the nodes of) the unconstrained XZ-plane S4.

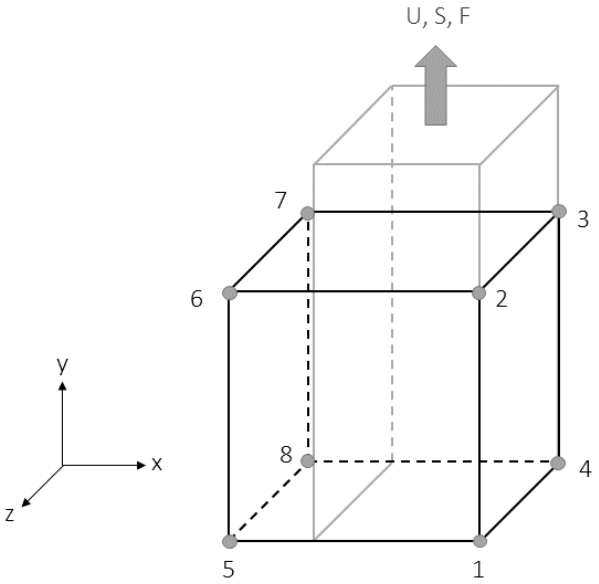

Plane	Nodes	BC
S1	1, 2, 3, 4	Fix X
S2	5, 6, 7, 8	
S3	1, 2, 5, 6	Fix Z
S4	2, 3, 6, 7	U, S, F
S5	3, 4, 7, 8	Fix Z
S6	1, 4, 5, 8	Fix Y

Figure 1: Schematic representation of the applied boundary conditions on the single element model. The nodes of the right YZ-plane S1 are fixed in the X-direction, the bottom XZ-plane S6 in the Y-direction, and both XY-planes S3 and S5 in the Z-direction, while a displacement (case U), stress (case S) or force (case F) is applied to (the nodes of) the top XZ-plane S4.

In case of a displacement boundary condition, case U, the deposition stretches are assumed to be unity, such that the homeostatic stresses are zero. In this case, the simulation goes through two steps. In the first step, the displacement is applied to reach a stretch of 1.5. Afterwards, the displacement is held constant, while (growth and) remodeling is enforced during 100 time steps, each corresponding to a time period of 10 days.

In case S, more steps are defined. First a homeostatic tensile stress of 0.100 MPa is gradually applied, while an initial guess for the corresponding deposition stretch tensor of the matrix material is defined as

$$\boldsymbol{G}^{elas} = \begin{bmatrix} 1/\sqrt{g_{zz}^{elas}} & 0 & 0 \\ 0 & 1/\sqrt{g_{zz}^{elas}} & 0 \\ 0 & 0 & g_{zz}^{elas} \end{bmatrix}, \tag{45}$$

with g_{zz}^{elas} the elastin deposition stretch in axial direction. If applicable, also a constant deposition stretch $g^{coll,i}$ in the fiber direction is applied. In the second step, a prestressing algorithm is applied, as explained

by Famaey et al. [17] and Maes et al. [11] in order to obtain the final $\boldsymbol{G}^{elas}$ for which the undeformed configuration ($\boldsymbol{F} = \boldsymbol{I}$) is in equilibrium with the externally applied homeostatic stress. Finally, in the third step, the stress is increased with 20% to 0.120 MPa, after which (growth and) remodeling is enforced during 100 time steps, each corresponding to a time period of 10 days.

In case F, the same steps are applied as in case S. The only difference is that a constant force is applied instead of a constant stress. A total homeostatic force of 250 N is considered, corresponding to a stress of 0.100 MPa in the reference configuration, given the dimensions of the element ($50 \times 50 \times 50$ mm^3), while the force is increased to 300 N at the beginning of the last step.

2.6. Step time convergence analysis

In the previously mentioned test cases, step times of 10 days are considered, the smallest possible for the classical constrained mixture theory, given the maximal amount of state dependent variables that can be defined in Abaqus. Assuming a $\boldsymbol{T}^j$ value of 101 days (see table 1), for a step time of 10 days, 69 cohorts of material are retained, such that all ignored cohorts are degraded for at least 99.9%, *i.e.* $\exp\left(-\frac{69+k}{101} \cdot 10\right) < 0.001$ for every $k = 1, 2, 3, ...$ In order to perform a step time convergence analysis, we rerun single-element case S with model E, assuming six larger step times of respectively 12, 15, 20, 30, 50 and 101 days. The step time convergence analysis for the homogenized constrained mixture theory is performed once, while that of the classical theory is performed twice: once when the number of retained cohorts is always equal to 69, and one when the number of cohorts is calculated in order to not consider cohorts that are degraded for more than 99.9%. In this latter case, only 58, 46, 34, 23, 13 or 6 cohorts are retained for the respective step times mentioned previously.

2.7. Application to arterial wall remodeling

Application of the (homogenized) constrained mixture theory is shown by modeling growth and remodeling of the arterial wall. Assuming axisymmetry of the problem, the geometry is represented by a quarter cylinder with an inner radius of 5 mm, thickness of 1.3 mm and length of 0.22 mm in the *in vivo* reference configuration. The finite element mesh is composed of 1920 C3D8 elements. In a first step, an intraluminal pressure of 10.0 kPa is applied as homeostatic load level, after which a prestressing algorithm is applied to obtain the homeostatic configuration [17, 11] in a second step. In the final third step, the pressure is increased to 15.0 kPa and 100 time steps of 10 days are considered for growth and remodeling, using model E defined in table 1. The fiber orientations are defined in every integration point based on the orientation of every element with respect to the centerline of the cylinder. Two fiber families in the axial

Model	A	B	C	D	E
$C_{10}M_0^{elas}/v_0^{elas}$ [MPa]	0.305	0.305	0.305	0.0305/0.8	0.0305/0.8
K [MPa]		6.10	6.10		0.610/0.8
$k_1 M_0^{coll}/v_0^{coll}$ [MPa]				0.0289/0.05	0.0289/0.05
k_2 [-]				1.23	1.23
α [rad]				$\pi/8$	$\pi/8$
$\rho^{elas}(0)$ [-]	1.0	1.0	1.0	0.8	0.8
$\rho^{coll,i}(0)$ [-]				0.05	0.05
g_{zz}^{elas} [-] (1)	1.2	1.2	1.2	1.2	1.2
$g^{coll,i}$ [-] (1)				1.1	1.1
T^{elas} [days]	101.0	101.0	101.0		
$T^{coll,i}$ [days]				101.0	101.0
$k_{\sigma+}^{elas}$ [-] or [MPa^{-1}] (2)			0.1		
$k_{\sigma-}^{elas}$ [-] or [MPa^{-1}] (2)			0.0		
$k_{\sigma+}^{coll,i}$ [-] or [MPa^{-1}] (2)					0.1
$k_{\sigma-}^{coll,i}$ [-] or [MPa^{-1}] (2)					0.0

Table 2
All parameter values used to test the model implementations A to E as defined in table 1. Notes: (1) These values only hold for the boundary conditions case S and F. In case U, all deposition stretches are unity. (2) These parameters are normally dimensionless due to the normalization of the stress difference in equations 11, 13 and 24. However, when the homeostatic stress is zero, the denominator is omitted, such that the dimension becomes MPa^{-1}.

and circumferential directions respectively are considered, as well as two symmetric fiber families oriented in the circumferential-axial plane with angle α with respect to the circumferential direction. Anisotropic growth defined with equation 7 is assumed, where $\boldsymbol{a}_g$ is a unit vector in the radial direction. This analysis is run using both the constrained mixture theory and its homogenized equivalent.

2.8. Parameters

All parameter values used to run all mentioned analyses are given in table 2. Note that not all parameters are applicable to all implementation cases defined in table 1.

3. Results

Ten different model implementations are tested for three different types of boundary conditions as explained in section 2.5. The results of all single-element test cases are reported in figure 2. In figure 2.I results of test case U are shown, where the YY-component of the Cauchy stress is depicted over time, while the stretch of the element is held constant.

Figure 2.II shows the results of test case S, where the normal Cauchy stress applied to the top XZ-surface of the element is held constant during remodeling. The figure shows the stretch of the element over time. The initial stretch at time 0 is caused by the tensile stress increase from the homeostatic level to the elevated level, while the further increase in stretch is due to remodeling.

	Case U		Case S		Case F	
Model	CM	HCM	CM	HCM	CM	HCM
A	34.6	4.1	39.3	5.8	46.6	5.2
B	34.1	3.9	39.5	6.7	45.9	5.3
C	35.1	3.7	36.7	5.3	41.1	4.7
D	42.1	4.3	60.8	6.9	49.4	6.2
E	40.5	3.9	61.1	7.1	55.5	5.3

Table 3
CPU time in seconds to run the 30 different test cases. Five models A to E are discerned as defined in table 1, with each a classical and homogenized version of the implementation, CM and HCM respectively. Three types of boundary conditions are tested: constant displacement (case U), stress (case S) or force (case F).

The results of test case F, where the normal force applied to the nodes of the top XZ-surface is held constant, are shown in figures 2.III and 2.IV, reporting the evolution of the stress and the stretch over time, respectively.

Table 3 gives an example of the CPU times necessary to run all different cases with an Intel Xeon Gold 6152, 2.10GHz processor (Intel Corp., Santa Clara, California, USA). These results clearly show the time-efficiency of the homogenized version of the constrained mixture theory.

The results of the step time convergence analysis are depicted in figure 3. In figures 3.I to 3.III, the stretch is shown over time for the different tested time step lengths. Remember that the step time convergence analysis for the classical constrained mixture theory is run twice, either always taking into account 69 cohorts (figure 3.I) or with an adapted number of cohorts (figure 3.II), while it is only run once for the homogenized constrained mixture theory (figure 3.III). The same results are represented differently in figure 3.IV, where the stretch level at 1000 days is plotted in function of the step time for the three same cases.

The results of the application to arterial growth and remodeling are shown in figure 4. The evolution of the circumferential stretch at the inner side of the wall, equal to one at homeostasis, is shown during the growth and remodeling period of 1000 days in figure 4.I. A clear dilatation of the artery can be observed, even with an increasing wall volume due to the increasing collagen density as observed in figure 4.II. Results are shown for both the constrained mixture theory and the homogenized equivalent. To run the full analysis, in the former case a CPU time of 3314.6 s was needed and 130.70 s in the latter case, again showing the time-efficiency of the homogenized theory.

4. Discussion

Looking at the results of the different test cases in detail provides meaningful insight in the mechanisms of remodeling defined by the constrained mixture theory and its homogenized equivalent. First looking

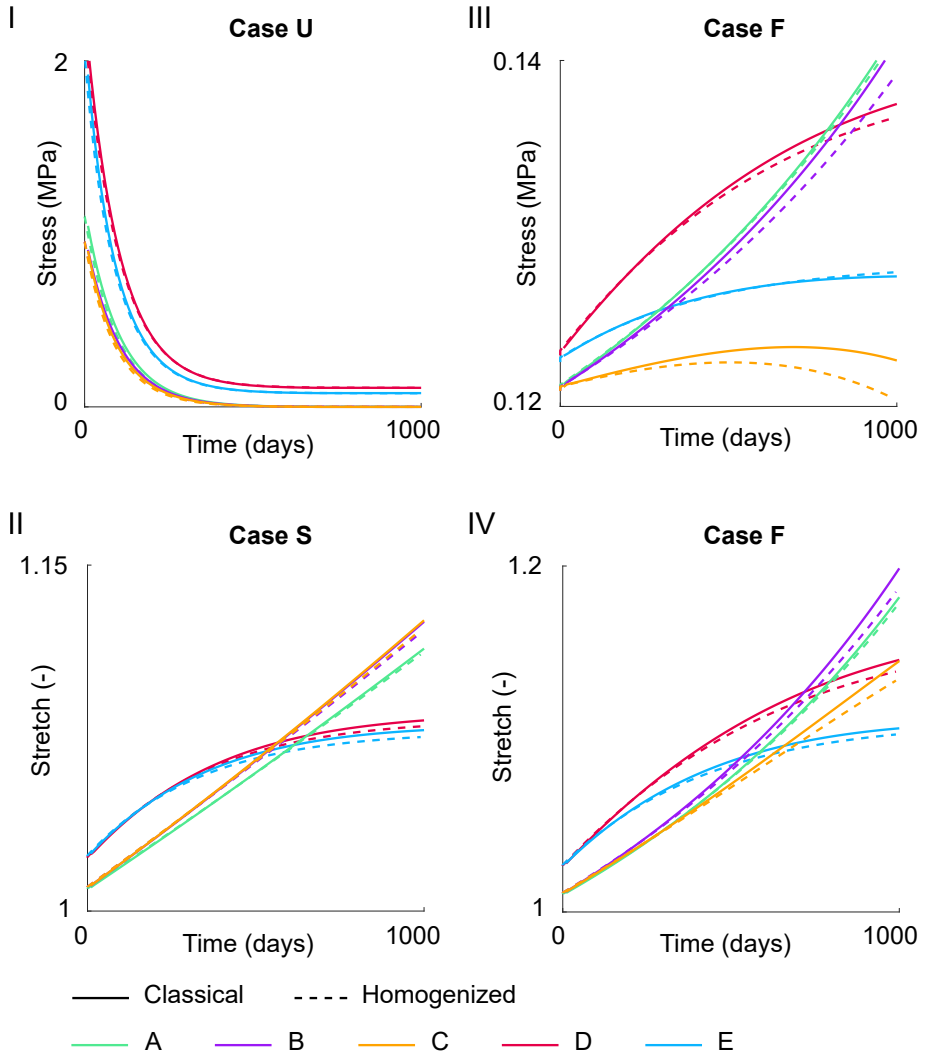

Figure 2: Results of the implemented models with the three test boundary condition test cases U, S and F. (I) YY-component of the Cauchy stress obtained with test case U over a period of 100 time steps or 1000 days. (II) Stretch in the Y-direction obtained with test case S over a period of 100 time steps or 1000 days. (III) YY-component of the Cauchy stress obtained with test case F over a period of 100 time steps or 1000 days. (IV) Stretch in the Y-direction obtained with test case F over a period of 100 time steps or 1000 days. In all cases, the full lines represent the results obtained with the classical constrained mixture theory, while the dashed lines represent the results obtained with the homogenized constrained mixture theory. The colors denoted with A to E correspond to the respective models A to E defined in table 1.

at the results of case U in figure 2.I, decreasing stresses are observed for a constant overstretching of the material. As also noted by Cyron et al. [8], there are clear mathematical similarities between the constrained mixture model and viscoelastic mechanical behavior, as figure 2.I shows typical stress relaxation-like curves. However, the physical interpretation is different. While classical viscoelastic behavior describes actual

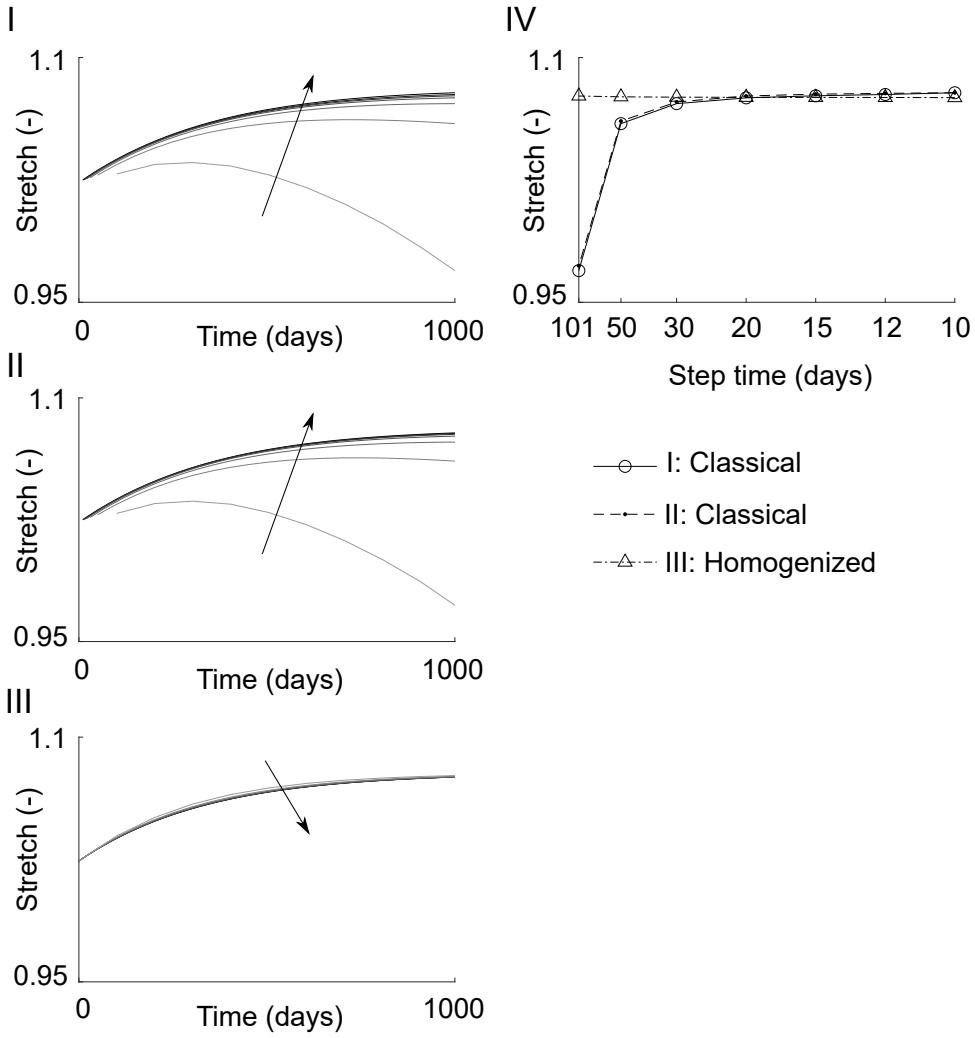

Figure 3: Results of the step time convergence analysis. Model E in combination with boundary conditions case S is run for different step times: 10, 12, 15, 20, 30, 50 and 101 days respectively. Stretches in the Y-direction over time are shown with (I) and (II) the classical constrained mixture theory and with (III) the homogenized constrained mixture theory. For the classical theory, the number of retained cohorts was either (I) always equal to 69, or (II) adapted to the step time. The arrows indicate the direction of convergence (towards shorter step times). (IV) shows the obtained stretches at day 1000 for the different cases I to III in function of the step time duration.

relaxation of the material, the constrained mixture theory relies on the principle that extant material is gradually replaced by new material deposited under a certain (often lower) prestress level.

In the specific tested case U, purely elastic material is initially stressed by applying a constant stretch. While all extant material that slowly degrades stays at this constant stress level, the newer material is

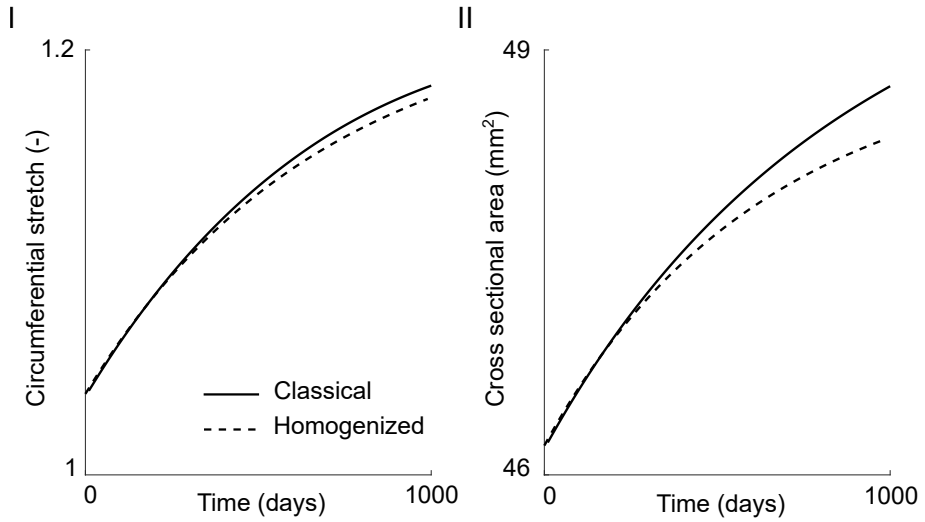

Figure 4: Results of the application to arterial wall growth and remodeling. (I) Circumferential stretch at the inner side of the wall over a period of 100 time steps or 1000 days. (II) Cross sectional area of the cylinder over a period of 100 time steps or 1000 days. In both cases, the full lines represent the results obtained with the classical constrained mixture theory, while the dashed lines represent the results obtained with the homogenized constrained mixture theory.

deposited at its homeostatic zero stress state. Therefore, the results of models A to C show a clear convergence to this zero stress state. In models D and E, the remaining stress after convergence can be fully attributed to the matrix material that does not renew, while the fiber stresses have converged to their zero stress homeostatic states.

The results of case S in figure 2.II show an initial limited stretch associated with the 20% increase of applied stress with respect to the homeostatic level in the undeformed reference configuration. However, this stretch level significantly increases over time, showing creep-like behavior, which can again be attributed to the replacement of highly stressed material by less stressed material. It is already clear that with models A to C, that exhibit a fairly linear stretch increase, a steady-state condition will never be reached, since this continuous replacement of material should always be compensated by increasing the overall stretch in order to balance the externally applied stress. Even with model C, a steady-state condition cannot be reached, since the mass increase leads to an equivalent increase in volume, hence increasing the reaction forces, but not the internal stresses.

Since models D and E include matrix material that does not remodel, but exhibits purely elastic behavior, a steady-state condition exists in these cases. The red and blue curves in figure 2.II show an evolving stretch to this steady-state, where all fibers are at their specific prestress level corresponding to a prestretch $g^{coll,i} = 1.1$ and where the matrix material is overstressed in order to compensate the 20% increase in

externally applied stress. Again in this case, including growth, and hence mass increase, does not affect the steady-state condition.

Overall, the results of case F are fairly similar to those of case S, although the internal stresses can increase due to the decreasing reaction surface with increasing stretch (see figure 2.III), leading to an even quicker deformation over time with models A and B. On the other hand, the growth in models C and E allows an increasing reaction surface, affecting the (existence of a) steady-state condition.

Figure 2 also shows a generally good correspondence between the constrained mixture model and its homogenized equivalent. Taking into account the slightly deviating behavior of the homogenized model in a nonlinear regime, as proven by Cyron et al. [8], we assume correct implementations of both models, given the nonlinear material behavior and large deformations. Performing a more detailed verification study is not straightforward, since both models are associated with different implementation difficulties, as explained in section 2.4, such that no ground truth results may be assumed.

Table 3 shows a clear time-efficiency in favor of the homogenized version of the theory for the same step time. Additionally, figure 3 shows that larger step times have a much smaller influence on the results, compared to the classical theory. Figures 3A and 3B also show that the number of retained cohorts beyond a degradation of 99.9% has only a very small influence on the results, compared to the influence of the step time.

Although validating the biological relevance of the constrained mixture theory is beyond the scope of this tutorial, getting insight in the behavior of the model when the material is subjected to these different types of loading is relevant, since soft tissues, such as tendons, ligaments, arteries, skin, etc. may also be subjected to various loading conditions *in vivo*. Along with the detailed description of the theoretical concepts and practical implementation methods, this should provide the reader with sufficient knowledge to apply these models to various and potentially unexplored applications. In order to further facilitate the application of these models to clinically relevant cases, a first example of growth and remodeling in the arterial wall is described here and the code is shared as supplementary material. The results of this example, depicted in figure 4, show an increasing arterial diameter over time due to hypertension.

In order to make an informed decision on the choice of both discussed theoretical frameworks, the main features of both are listed in table 4.

	Classical	Homogenized
1	Agreement with HCM in linear regime [8]	Agreement with CM in linear regime [8]
2	Large storage space required	Small storage space required
3	Intuitive theoretical concept	Complex theoretical concept
4	Complex implementation for 1D fiber material and 3D material	Simple implementation for 1D fiber material and complex implementation for 3D material
5	Simple extension to new material definitions	Complex extension to new material definitions
6	Long run time	Short run time
7	High sensitivity to step time	Low sensitivity to step time

Table 4
Comparison of the main advantages and disadvantages of the classical (CM) and homogenized (HCM) constrained mixture models.

5. Conclusion

To conclude, a few practical guidelines are proposed in order to further facilitate the use of these models. To use the classical constrained mixture theory:

1. Determine the step time based on the characteristic decay time T^j of the growing and remodeling material j. As a general rule of thumb, it should hold that $\frac{T^j}{\Delta s} \geq 10$. In case multiple types of materials are considered with a different T^j, choose the most stringent condition.
2. Based on the step time and the characteristic decay time, determine the number of cohorts n^j of the material j that will be retained. Choose n^j such that the first ignored cohort becomes insignificant, and that it is for example degraded for at least 99.9%, such that $n^j > \frac{-T^j}{\Delta s} \cdot \log(0.001)$.
3. Calculate the number of variables to be stored. These include nine times n^j variables to store deformation gradient components, the number of material groups, e.g. fiber families, times n^j variables to store the rates of deposition $m^j(\tau)$ and, if necessary, the same number of variables to store the time-dependent degradation parameters $K^j_{_}$. As an example, this amounts to $9 \cdot 69 + 4 \cdot 69 = 897$ variables in the models D and E of the present study (69 cohorts of four fiber families). If the obtained number is deemed unfeasible, the previous items 1 and 2 should be revisited or a switch to the homogenized mixture theory should be made.
4. As explained in section 2.4.1, use a trapezoidal rule to approximate the integrals of equations 1 and 4.
5. In case of a stress-dependent current rate of deposition $m^j(s)$, implement an iterative loop, updating $m^j(s)$ at every iteration.

To use the homogenized constrained mixture theory:

1. Determine the step time based on the characteristic decay time T^j of the growing and remodeling material j. As a general rule of thumb, it should hold that $\frac{T^j}{\Delta s} \geq 4$. In case multiple types of materials are considered with a different T^j, choose the most stringent condition.
2. Based on the constitutive model of the considered remodeling material, analytically derive the stiffness tensor $\left(\frac{\partial \boldsymbol{\sigma}^j}{\partial \boldsymbol{F}_e^j}\right)_{\boldsymbol{F},\boldsymbol{F}_g=const}$ (or use a symbolic solver) and transform to Voigt notation. Determine the rank of the obtained matrix, that should be in a range from 1 to 6.
3. Define the remodeling deformation gradient $\boldsymbol{F}_r^j$, such that the number of unknown components is equal to the previously obtained rank. Examples can be found in section 2.4.2.
4. Based on the previous point, in case no analytical solution of equation 20, similar to equation 41, can be found, use a numerical solver to solve the system of nonlinear equations. Note that some methods require the Jacobian matrix of the problem that can be derived analytically or with a symbolic solver.

A. Derivation of equations 29, 40, 42 and 44

In order to derive equations 29, we calculate the derivatives of the strain energy density functions with respect to the invariants (equations A.1 to A.4), as well as the derivatives of the invariants with respect to the elastic parts of the deformation gradient (equations A.5 to A.8) and with respect to the total deformation gradient (equations A.9 to A.11):

$$\frac{\partial W^{elas}}{\partial \bar{I}_1^{elas}} = \boldsymbol{C}_{10}, \tag{A.1}$$

$$\frac{\partial W^{elas}}{\partial \boldsymbol{J}_e^{elas}} = \boldsymbol{K}\left(\boldsymbol{J}_e^{elas} - 1\right), \tag{A.2}$$

$$\frac{\partial W^{coll,i}}{\partial I_4^{coll,i}} = k_1\left(I_4^{coll,i} - 1\right)\exp\left\{k_2\left(I_4^{coll,i} - 1\right)^2\right\}, \tag{A.3}$$

$$\frac{\partial^2 W^{coll,i}}{\left(\partial I_4^{coll,i}\right)^2} = k_1\left[1 + 2k_2\left(I_4^{coll,i} - 1\right)^2\right]\exp\left\{k_2\left(I_4^{coll,i} - 1\right)^2\right\}, \tag{A.4}$$

$$\frac{\partial \boldsymbol{J}_e^{elas}}{\partial \boldsymbol{F}_e^{elas}} = \boldsymbol{J}_e^{elas}(\boldsymbol{F}_e^{elas})^{-T}, \tag{A.5}$$

$$\frac{\partial I_1^{elas}}{\partial \boldsymbol{F}_e^{elas}} = 2\boldsymbol{F}_e^{elas}, \tag{A.6}$$

$$\frac{\partial I_4^{coll,i}}{\partial \boldsymbol{F}_e^{coll,i}} = 2\left(\boldsymbol{F}_e^{coll,i}\boldsymbol{M}^i\right)\otimes\boldsymbol{M}^i, \tag{A.7}$$

$$\frac{\partial \bar{I}_1^{elas}}{\partial \boldsymbol{F}_e^{elas}} = (J_e^{elas})^{-2/3}\left(2\boldsymbol{F}_e^{elas} - \frac{2}{3}(\boldsymbol{F}_e^{elas})^{-T} I_1^{elas}\right), \tag{A.8}$$

$$\frac{\partial J_e^{elas}}{\partial \boldsymbol{F}}\boldsymbol{F}^T = \frac{\partial J_e^{elas}}{\partial \boldsymbol{F}_e^{elas}} : \frac{\partial \boldsymbol{F}_e^{elas}}{\partial \boldsymbol{F}}\boldsymbol{F}^T = J_e^{elas}\boldsymbol{I} = \frac{J}{J_g}\boldsymbol{I}, \tag{A.9}$$

$$\frac{\partial \bar{I}_1^{elas}}{\partial \boldsymbol{F}}\boldsymbol{F}^T = \frac{\partial \bar{I}_1^{elas}}{\partial \boldsymbol{F}_e^{elas}} : \frac{\partial \boldsymbol{F}_e^{elas}}{\partial \boldsymbol{F}}\boldsymbol{F}^T = 2\bar{\boldsymbol{B}}_e^{elas} - \frac{2}{3}\bar{I}_1^{elas}\boldsymbol{I}, \tag{A.10}$$

$$\frac{\partial I_4^{coll,i}}{\partial \boldsymbol{F}}\boldsymbol{F}^T = \frac{\partial I_4^{coll,i}}{\partial \boldsymbol{F}_e^{coll,i}} : \frac{\partial \boldsymbol{F}_e^{coll,i}}{\partial \boldsymbol{F}}\boldsymbol{F}^T = 2\left(\boldsymbol{F}_e^{coll,i}\boldsymbol{M}^i\right) \otimes \left(\boldsymbol{F}_e^{coll,i}\boldsymbol{M}^i\right). \tag{A.11}$$

Therefore, the Cauchy stresses are obtained as

$$\begin{aligned}
\boldsymbol{\sigma}^{elas} &= \frac{\rho^{elas}}{\phi^{elas}\boldsymbol{J}}\frac{\partial W^{elas}}{\partial \boldsymbol{F}}\boldsymbol{F}^T \\
&= \frac{\rho^{elas}}{\phi^{elas}\boldsymbol{J}}\left(\frac{\partial W^{elas}}{\partial \bar{I}_1^{elas}}\frac{\partial \bar{I}_1^{elas}}{\partial \boldsymbol{F}} + \frac{\partial W^{elas}}{\partial J_e^{elas}}\frac{\partial J_e^{elas}}{\partial \boldsymbol{F}}\right)\boldsymbol{F}^T \\
&= 2C_{10}\frac{\rho^{elas}}{\phi^{elas}\boldsymbol{J}}\left(\bar{\boldsymbol{B}}_e^{elas} - \frac{1}{3}\bar{I}_1^{elas}\boldsymbol{I}\right) + \frac{K\rho^{elas}}{\phi^{elas}\boldsymbol{J}_g}\left(J_e^{elas} - 1\right)\boldsymbol{I},
\end{aligned} \tag{A.12}$$

and

$$\begin{aligned}
\boldsymbol{\sigma}^{coll,i} &= \frac{\rho^{coll,i}}{\phi^{coll,i}\boldsymbol{J}}\frac{\partial W^{coll,i}}{\partial \boldsymbol{F}}\boldsymbol{F}^T \\
&= \frac{\rho^{coll,i}}{\phi^{coll,i}\boldsymbol{J}}\frac{\partial W^{coll,i}}{\partial I_4^{coll,i}}\frac{\partial I_4^{coll,i}}{\partial \boldsymbol{F}}\boldsymbol{F}^T \\
&= 2k_1\frac{\rho^{coll,i}}{\phi^{coll,i}\boldsymbol{J}}\left(I_4^{coll,i} - 1\right)\exp\left\{k_2\left(I_4^{coll,i} - 1\right)^2\right\}\left(\boldsymbol{F}_e^{coll,i}\boldsymbol{M}^i\right) \otimes \left(\boldsymbol{F}_e^{coll,i}\boldsymbol{M}^i\right).
\end{aligned} \tag{A.13}$$

In order to derive equations 40, 42 and 44, we need, in index notation,

$$\frac{\partial\left[\left(\boldsymbol{F}_e^{coll,i}\right) \otimes \left(\boldsymbol{F}_e^{coll,i}\right)\right]_{ij}}{\partial\left(\boldsymbol{F}_e^{coll,i}\right)_{kl}} = \left[\delta_{ik}\left(\boldsymbol{F}_e^{coll,i}\boldsymbol{M}^i\right)_j\left(\boldsymbol{M}^i\right)_l + \delta_{jk}\left(\boldsymbol{F}_e^{coll,i}\boldsymbol{M}^i\right)_i\left(\boldsymbol{M}^i\right)_l\right], \tag{A.14}$$

$$\frac{\partial\left(\boldsymbol{B}_e^{elas}\right)_{ij}}{\partial\left(\boldsymbol{F}_e^{elas}\right)_{kl}} = \delta_{ik}(\boldsymbol{F}_e^{elas})_{jl} + \delta_{jk}(\boldsymbol{F}_e^{elas})_{il}, \tag{A.15}$$

$$\frac{\partial\left(\bar{\boldsymbol{B}}_e^{elas}\right)_{ij}}{\partial\left(\boldsymbol{F}_e^{elas}\right)_{kl}} = (J_e^{elas})^{-2/3}\left(\delta_{ik}(\boldsymbol{F}_e^{elas})_{jl} + \delta_{jk}(\boldsymbol{F}_e^{elas})_{il} - \frac{2}{3}(\boldsymbol{F}_e^{elas\,-T})_{kl}(\boldsymbol{B}_e^{elas})_{ij}\right). \tag{A.16}$$

Therefore,

$$\begin{aligned}\left(\frac{\partial \boldsymbol{\sigma}^{coll,i}}{\partial \boldsymbol{F}_e^{coll,i}}\right)_{ijkl}^{\boldsymbol{F},\boldsymbol{F}_g=const} =& \frac{2\rho^{coll,i}}{\phi^{coll,i}J}\frac{\partial^2 W^{coll,i}}{\left(\partial I_4^{coll,i}\right)^2}\frac{\partial I_4^{coll,i}}{\partial\left(\boldsymbol{F}_e^{coll,i}\right)_{ij}}\left(\boldsymbol{F}_e^{coll,i}\right)_k\left(\boldsymbol{F}_e^{coll,i}\right)_l \\ &+\frac{2\rho^{coll,i}}{\phi^{coll,i}J}\frac{\partial W^{coll,i}}{\partial I_4^{coll,i}}\frac{\partial\left[\left(\boldsymbol{F}_e^{coll,i}\right)\otimes\left(\boldsymbol{F}_e^{coll,i}\right)\right]_{ij}}{\partial\left(\boldsymbol{F}_e^{coll,i}\right)_{kl}} \\ =& \frac{4\rho^{coll,i}}{\phi^{coll,i}J}k_1\left[1+2k_2\left(I_4^{coll,i}-1\right)^2\right]\exp\left\{k_2\left(I_4^{coll,i}-1\right)^2\right\} \\ &\cdot\left(\boldsymbol{F}_e^{coll,i}\boldsymbol{M}^i\right)_i\left(\boldsymbol{F}_e^{coll,i}\boldsymbol{M}^i\right)_j\left(\boldsymbol{F}_e^{coll,i}\boldsymbol{M}^i\right)_k\left(\boldsymbol{M}^i\right)_l \\ &+\frac{2\rho^{coll,i}}{\phi^{coll,i}J}k_1\left(I_4^{coll,i}-1\right)\exp\left\{k_2\left(I_4^{coll,i}-1\right)^2\right\} \\ &\cdot\left[\delta_{ik}\left(\boldsymbol{F}_e^{coll,i}\boldsymbol{M}^i\right)_j\left(\boldsymbol{M}^i\right)_l+\delta_{jk}\left(\boldsymbol{F}_e^{coll,i}\boldsymbol{M}^i\right)_i\left(\boldsymbol{M}^i\right)_l\right],\end{aligned} \tag{A.17}$$

for equation 42,

$$\begin{aligned}\left(\frac{\partial \boldsymbol{\sigma}^{elas}}{\partial \boldsymbol{F}_e^{elas}}\right)_{ijkl}^{\boldsymbol{F},\boldsymbol{F}_g=const} =& 2C_{10}\frac{\rho^{elas}}{\phi^{elas}J}\left(\frac{\partial\left(\bar{\boldsymbol{B}}_e^{elas}\right)_{ij}}{\partial\left(\boldsymbol{F}_e^{elas}\right)_{kl}}-\frac{1}{3}\delta_{ij}\frac{\partial \bar{I}_1^{elas}}{\partial\left(\boldsymbol{F}_e^{elas}\right)_{kl}}\right)+K\frac{\rho^{elas}}{\phi^{elas}J_g}\delta_{ij}\frac{\partial J_e^{elas}}{\partial\left(\boldsymbol{F}_e^{elas}\right)_{kl}} \\ =& 2C_{10}\frac{\rho^{elas}}{\phi^{elas}J}\left[(J_e^{elas})^{-2/3}\left(\delta_{ik}\left(\boldsymbol{F}_e^{elas}\right)_{jl}+\delta_{jk}\left(\boldsymbol{F}_e^{elas}\right)_{il}-\frac{2}{3}\delta_{ij}\left(\boldsymbol{F}_e^{elas}\right)_{kl}\right)\right. \\ &\left.+\frac{2}{3}(J_e^{elas})^{-2/3}\left(\boldsymbol{F}_e^{elas\,-T}\right)_{kl}\left(-\left(\boldsymbol{B}_e^{elas}\right)_{ij}+\frac{1}{3}I_1^{elas}\delta_{ij}\right)\right] \\ &+\frac{\rho^{elas}}{\phi^{elas}J_g}KJ_e^{elas}\left(\boldsymbol{F}_e^{elas}\right)_{kl}\delta_{ij},\end{aligned} \tag{A.18}$$

and for equation 44,

$$\begin{aligned}\left(\frac{\partial \boldsymbol{\sigma}^{elas}}{\partial \boldsymbol{F}_e^{elas}}\right)_{ijkl}^{\boldsymbol{F},\boldsymbol{F}_g=const} &= 2C_{10}\frac{\rho^{elas}}{\phi^{elas}}\left(\frac{\partial(\boldsymbol{B}_e^{elas})_{ij}}{\partial(\boldsymbol{F}_e^{elas})_{kl}}-\frac{1}{3}\delta_{ij}\frac{\partial I_e^{elas}}{\partial(\boldsymbol{F}_e^{elas})_{kl}}\right) \\ &= 2C_{10}\frac{\rho^{elas}}{\phi^{elas}}\left(\delta_{ik}\left(\boldsymbol{F}_e^{elas}\right)_{jl}+\delta_{jk}\left(\boldsymbol{F}_e^{elas}\right)_{il}-\frac{2}{3}\delta_{ij}\left(\boldsymbol{F}_e^{elas}\right)_{kl}\right).\end{aligned} \tag{A.19}$$

Supplementary material

All Abaqus files, including UMAT subroutines and input files, can be downloaded from `https://bme-soft-tissue.pages.gitlab.kuleuven.be/Constrained_mixture_GR_models`.

Acknowledgements

This work was funded by the Research Foundation-Flanders through a doctoral fellowship for fundamental research (11A6519N). We are also grateful to Dr. S. Jamaleddin Mousavi and Dr. Felipe Sempértegui (Mines Saint-Étienne, France), and Dr. Julie Vastmans and ir. Thibault Vervenne (KU Leuven, Belgium) for their insights in this work.

Competing interests

The authors have no competing interests to declare.

CRediT authorship contribution statement

Lauranne Maes: Conceptualization, Software, Validation, Writing - Original Draft, Visualization, Funding acquisition. **Nele Famaey:** Conceptualization, Writing - Review and Editing, Supervision, Funding acquisition.

References

[1] H. Wolinsky and S. Glagov. A lamellar unit of aortic medial structure and function in mammals. *Circulation research*, 20(1):99–111, 1967.

[2] R. E. Shadwick. Mechanical design in arteries. *Journal of Experimental Biology*, 202(23):3305–3313, 1999.

[3] J. F. Eichinger, L. J. Haeusel, D. Paukner, R. C. Aydin, J. D. Humphrey, and C. J. Cyron. Mechanical homeostasis in tissue equivalents: a review. *Biomechanics and Modeling in Mechanobiology*, 20(3):833–850, 2021.

[4] J. D. Humphrey and K. R. Rajagopal. A Constrained Mixture Model For Growth And Remodelling Of Soft Tissues. *Mathematical Models and Methods in Applied Sciences*, 12(03):407–430, 2002.

[5] J. Ferruzzi, M. J. Collins, A. T. Yeh, and J. D. Humphrey. Mechanical assessment of elastin integrity in fibrillin-1-deficient carotid arteries: Implications for Marfan syndrome. *Cardiovascular Research*, 92(2):287–295, 2011.

[6] C. Bellini, J. Ferruzzi, S. Roccabianca, E. S. Di Martino, and J. D. Humphrey. A Microstructurally Motivated Model of Arterial Wall Mechanics with Mechanobiological Implications. *Annals of Biomedical Engineering*, 42(3):488–502, mar 2014.

[7] J. D. Humphrey. Constrained Mixture Models of Soft Tissue Growth and Remodeling – Twenty Years After. *Journal of Elasticity*, 145(1-2):49–75, 2021.

[8] C. J. Cyron, R. C. Aydin, and J. D. Humphrey. A homogenized constrained mixture (and mechanical analog) model for growth and remodeling of soft tissue. *Biomechanics and Modeling in Mechanobiology*, 15(6):1389–1403, 2016.

[9] F. A. Braeu, A. Seitz, R. C. Aydin, and C. J. Cyron. Homogenized constrained mixture models for anisotropic volumetric growth and remodeling. *Biomechanics and Modeling in Mechanobiology*, 16(3):889–906, 2017.

[10] S. J. Mousavi, S. Farzaneh, and S. Avril. Patient-specific predictions of aneurysm growth and remodeling in the ascending thoracic aorta using the homogenized constrained mixture model. *Biomechanics and Modeling in Mechanobiology*, 18(6):1895–1913, 2019.

[11] L. Maes, H. Fehervary, J. Vastmans, S. J. Mousavi, S. Avril, and N. Famaey. Constrained mixture modeling affects material parameter identification from planar biaxial tests. *Journal of the Mechanical Behavior of Biomedical Materials*, 95:124–135, 2019.

[12] A. Ghavamian, S. J. Mousavi, and S. Avril. Computational Study of Growth and Remodeling in Ascending Thoracic Aortic Aneurysms Considering Variations of Smooth Muscle Cell Basal Tone. *Frontiers in Bioengineering and Biotechnology*, 8, 2020.

[13] S. Baek, K. R. Rajagopal, and J. D. Humphrey. A theoretical model of enlarging intracranial fusiform aneurysms. *Journal of Biomechanical Engineering*, 128(1):142–149, 2006.

[14] E. K. Rodriguez, A. Hoger, and A. D. McCulloch. Stress-dependent finite growth in soft elastic tissues. *Journal of Biomechanics*, 27(4):455–467, 1994.

[15] A. Valentín, J. D. Humphrey, and G. A. Holzapfel. A finite element-based constrained mixture implementation for arterial growth, remodeling, and adaptation: Theory and numerical verification. *International Journal for Numerical Methods in Biomedical Engineering*, 29(8):822–849, 2013.

[16] W. H. Press, S. A. Teukolsky, W. T. Vetterling, and B. P. Flannery. *Numerical Recipes in Fortran: The Art of Scientific Computing*. Cambridge University Press, 1993.

[17] N. Famaey, J. Vastmans, H. Fehervary, L. Maes, E. Vanderveken, F. Rega, S. J. Mousavi, and S. Avril. Numerical simulation of arterial remodeling in pulmonary autografts. *ZAMM - Journal of Applied Mathematics and Mechanics / Zeitschrift für Angewandte Mathematik und Mechanik*, 98(12):2239–2257, 2018.